NBO, FUKUI FUNCTIONS, RDG, ELF, LOL, AND MESP ANALYSIS OF 2-4-DIAMINO-6-DIALLYLAMINO-1,3,5-TRIAZINE USING DFT

Annu[1], B. S. Yadav[2], Jayant Teotia[3]*

Abstract

In the present work, various computational tools have been used for the analysis of 2-4-diamino-6-diallylamino-1,3,5-triazine (DDA-1,3,5T) with the help of density functional theory (DFT) using the B3LYP method at 6-311++G(d, p) and cc-p VDZ basis sets. The analysis of Natural bond orbitals (NBO) helped in studying the interactions between acceptor and donor orbitals for DDA-1,3,5T at 6-311++G(d, p) level. The study of non-covalent interactions helped in analyzing reduced density gradient. The chemical reactivity and selectivity for a local reactivity site have been analyzed using Fukui functions. The topological characteristics such as the Localized Orbital Locator and the Electron Localisation Function of DDA-1,3,5T are studied using Multiwfn software. DFT calculations are carried out to study the molecular electrostatic potential of DDA-1,3,5T with the help of the Gaussian09W program.

Keywords: DDA-1,3,5T, NBO, RDG, Fukui, ELF-LOL

[1,2,3]*Molecular Spectroscopy and Biophysics Laboratory, Department of Physics, Deva Nagri College, Meerut-250002, Uttar Pradesh, India. [3]Email: jayant.phy@gmail.com

***Corresponding Author:** Jayant Teotia

*Molecular Spectroscopy and Biophysics Laboratory, Department of Physics, Deva Nagri College, Meerut-250002, Uttar Pradesh, India. Email: jayant.phy@gmail.com

DOI: 10.48047/ecb/2023.12.si5a.0401

1. Introduction

Triazine is an organic compound having variety of uses in the industrial and medicinal fields. A novel triazine (R_1-MOF), which acts as a flame retardant and suppresses the release of smoke, has been synthesized to lower the toxicity of epoxy resin that polluted the environment [1]. The addition of an electron-affluent ketone group to the triazine-based covalent organic frameworks results in the narrowing of the band gap due to the hike in ketone content and these covalent organic framework-based catalysts have great potential in enhancing the photocatalytic degradation of the organic pollutants [2]. The substituted triazine derivatives have been used to synthesize hetero-cycle in the form of intermediates and reagents [3]. A triazine-based microporous organic network (TMON) is an excellent environmental adsorbent because of its recyclability and large surface area. The contaminants such as nadifloxacin and flumequine are effectively adsorbed by highly adaptable and stable TMON [4]. The s-triazine derivatives are endowed with higher selectivity and efficacy in blocking mechanisms owing to which they act as epidermal growth factor kinase inhibitors, thymidine phosphorylase, and protein kinase paving the way for the medicines to fight against breast cancer and tumours [5–7]. The incorporation of nanoparticles of calcium citrate and biguanide-based synthesis substituted triazine derivatives exhibited anticancer activity [8]. The effects of prototropic tautomerism on s-triazines in optoelectronics to study its NLO properties have also been reported [9].

Owing to various applications and utilities of the triazine compounds, the 2-4-diamino-6-diallyl amino-1,3,5-triazine (DDA-1,3,5T) molecule has been chosen for the computational investigations assisted by density functional theory (DFT) using B3LYP/6-311++G (d, p) and B3LYP/cc-p VDZ basis sets.

2. Computational Details

The computational investigations on DDA-1,3,5T have been carried out using different computational programs with the help of 6-311++G(d, p) and cc-p VDZ basis sets by employing B3LYP method assisted by the Gaussian 09W [10] and Gauss view 6 [11] program to obtain the optimized structure of the molecule. The local reactivity descriptors, Electron Localisation Function (ELF), Localized Orbital Locator (LOL), and Reduced Density Gradient (RDG) have been examined using Multiwfn [12] and VMD [13] programs. Natural bond orbitals (NBO) and Molecular Electrostatic Potential (MEP) have been evaluated using DFT.

3. Results and Discussion

3.1 Structural parameters and geometry of the molecule

The DDA-1,3,5T molecule possesses Cs symmetry and the labelled molecular structure is illustrated in Figure 1 along with the numbering of atoms where amino and allylamino groups are bonded with the triazine ring. The molecular structure of DDA-1,3,5T is optimized using the B3LYP method at 6-311++G(d, p) and cc-p VDZ levels to calculate the structural parameters as depicted in Table 1. The bond length between C–N atoms ranges from 1.338 Å to 1.467 Å while for N–H atoms are almost equal and vary from 1.006 Å to 1.006 Å. The bond length between C–C atoms is of the order of 1.33 Å for C12–C13 and C14–C15 which is less due to double bond as compared to single bonds between C10–C12 and C11–C14 which is of the order of 1.5 Å. The C–H bond length is in the range of 1.084 Å to 1.095 Å. The triazine ring has six possible bond angles where three alternate bond angles at N1, N3, and N5 positions are in the range of 113° to 114° while the other three alternate bond angles at C2, C4, and C6 positions are in the range of 124.8° to 126.3°. The two amino groups at the second and fourth place of the triazine ring have bond angles (N1–C2–N7, N3–C2–N7, N3–C4–N9 and N5–C4–N9) of the order of 116°. The bond angles (C2–N7–H16, C2–N7–H17, C4–N9–H18 and C4–N9–H19) of the amino group are of the order of 117°. The bond angles (H16–N7–H17 and H18–N9–H19) of the amino group are of the order of 119°. The bond angles between C–C–H atoms of the two allyl groups positioned at N8 vary from 110° to 121°. The bond angles between H–C–H atoms of the two allyl groups vary from 107° to 116°. The bond angles between C–C–C atoms of the two allyl groups are of the order of 124°. The computed values of the structural parameters of the DDA-1,3,5T compound are almost equal for both basis sets.

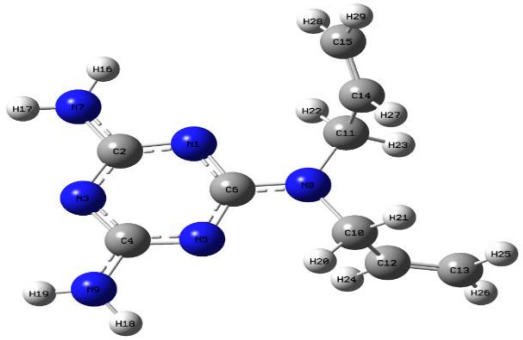

Figure 1. Structure of the DDA-1,3,5T molecule.

Table 1. Computed optimized structural parameters of DDA-1,3,5T molecule.

Bond Length (Å)	B3LYP/ 6-311G++(d, p)	B3LYP/ cc-p VDZ	Bond Angle (°)	B3LYP/ 6-311G++(d, p)	B3LYP/ cc-p VDZ
C2–N1	1.338	1.343	C2–N1–C6	114.4	114.0
C6–N1	1.345	1.347	N3–C2–N1	126.4	126.8
N3–C2	1.341	1.345	N7–C2–N1	116.9	116.7
C2–N7	1.362	1.365	N7–C2–N3	116.7	116.5
C4–N3	1.340	1.344	C4–N3–C2	113.5	113.1
N5–C4	1.338	1.343	N5–C4–N3	126.3	126.7
N9–C4	1.362	1.366	N9–C4–N3	116.7	116.6
C6–N5	1.347	1.349	N9–C4–N5	116.9	116.7
N8–C6	1.364	1.370	C6–N5–C4	114.5	114.0
H16–N7	1.006	1.012	N5–C6–N1	124.9	125.4
H17–N7	1.006	1.012	N8–C6–N1	117.6	117.3
N8–C10	1.466	1.464	N8–C6–N5	117.6	117.3
N8–C11	1.467	1.465	C2–N7–H16	117.7	117.0
N9–H18	1.006	1.012	C2–N7–H17	117.6	116.8
N9–H19	1.006	1.012	H16–N7–H17	119.0	118.5
C10–C12	1.506	1.507	C10–N8–C6	121.3	121.2
C10–H20	1.090	1.098	C11–N8–C6	121.2	120.9
C10–H21	1.095	1.103	C10–N8–C11	117.5	117.9
C11–C14	1.508	1.510	C4–N9–H18	118.0	116.8
C11–H22	1.089	1.096	C4–N9–H19	117.8	116.5
C11–H23	1.096	1.104	H18–N9–H19	119.3	118.2
C13–C12	1.331	1.336	N8–C10–C12	112.4	112.4
H24–C12	1.088	1.097	N8–C10–H20	107.5	107.0
H25–C13	1.087	1.095	N8–C10–H21	108.7	109.1
H26–C13	1.084	1.093	C12–C10–H20	110.0	109.9
C15–C14	1.330	1.335	C12–C10–H21	110.1	110.1
H27–C14	1.089	1.097	H20–C10–H21	108.1	108.3
H28–C15	1.086	1.094	N8–C11–C14	113.0	112.9
H29–C15	1.084	1.093	N8–C11–H22	108.9	108.6
			N8–C11–H23	106.9	106.9
			C14–C11–H22	110.1	110.0
			C14–C11–H23	109.9	110.0
			H22–C11–H23	107.9	108.2
			C13–C12–C10	124.6	124.8
			C10–C12–H24	115.3	115.1
			H24–C12–C13	120.1	120.1
			C12–C13–H25	121.6	121.4
			H26–C13–C12	121.8	121.7
			H26–C13–H25	116.7	116.9
			C15–C14–C11	124.3	124.3
			C11–C14–H27	116.2	116.3
			C15–C14–H27	119.5	119.4
			H28–C15–C14	121.4	121.2
			H29–C15–C14	121.7	121.6
			H28–C15–H29	116.9	117.2

3.2 Natural Bond Orbitals (NBO)

NBO of a molecule enables us to understand Lewis acid/Lewis base interactions, stabilizing reactions between occupied and unoccupied orbitals, bond order, hybridization, and intra-molecular conjugative interactions resulting in the strengthening of the bonds [14]. Lewis orbitals are the filled ones acting as donors while non-Lewis orbitals are unoccupied orbitals and act as an acceptor [15,16]. The Lewis and non-Lewis atomic orbitals overlap to form stabilized molecular orbitals with lower energy states due to the delocalization of electrons. The decrease in the amount of energy is called the stabilization energy ΔE_{ij} and is given by

$$\Delta E_{ij} = q_i \frac{F(i,j)^2}{\varepsilon_j - \varepsilon_i}$$

where $\varepsilon_j - \varepsilon_i$ is the difference in energy between the acceptor (j) and the donor (i) NBOs, F(i,j) is the Fock matrix element between i and j NBOs.

The second-order perturbation theory investigations of the Fock matrix in NBO that helps in predicting the interactivities between donor-acceptor for DDA-1,3,5T is computed and is listed in Table 2.

Table 2. NBO investigations of DDA-1,3,5T computed at 6-311++G(d,p) level.

Donor NBO(i)	ED/e	Energy ε_i	Acceptor NBO(j)	Energy ε_j	ΔE_{ij} [a] kcal/mol	$\varepsilon_j-\varepsilon_i$ [b] (a.u.)	F(i,j) [c] (a.u.)
σN1–C6	1.97959	−0.82175	σ*C2–N7	0.46825	4.29	1.29	0.067
πN1–C6	1.73733	−0.29480	π*N1–C6	0.0052	4.17	0.30	0.033
			π*C2–N3	0.0052	44.22	0.30	0.108
			π*C4–N5	0.0052	4.07	0.30	0.033
σC2–N3	1.98232	−0.82486	σ*C4–N9	0.46514	4.44	1.29	0.068
πC2–N3	1.74129	−0.29581	π*C2–N3	0.00419	4.31	0.30	0.034
			π*C4–N5	0.00419	43.79	0.30	0.108
σN3–C4	1.98228	−0.82529	σ*C2–N7	0.46471	4.42	1.29	0.068
πC4–N5	1.75466	−0.29846	π*N1–C6	0.00154	41.26	0.30	0.106
σN5–C6	1.97980	−0.82122	σ*C4–N9	0.46878	4.31	1.29	0.067
σN7–H16	1.98775	−0.66175	σ*C2–N3	0.52825	4.27	1.19	0.064
σN7–H17	1.98773	−0.66131	σ*N1–C2	0.53869	4.40	1.20	0.065
σN9–H18	1.98807	−0.66346	σ*N3–C4	0.52654	4.27	1.19	0.064
σN9–H19	1.98792	−0.66271	σ*C4–N5	0.53729	4.41	1.20	0.065
LP(1)N1	1.90046	−0.34416	σ*C2–N3	0.52584	12.15	0.87	0.093
			σ*N5–C6	0.51584	11.85	0.86	0.092
LP(1)N3	1.90757	−0.34981	σ*N1–C2	0.53019	11.84	0.88	0.093
			σ*C4–N5	0.53019	11.86	0.88	0.093
LP(1)N5	1.90018	−0.34681	σ*N1–C6	0.52319	11.69	0.87	0.091
			σ*N3–C4	0.53319	12.03	0.88	0.093
LP(1)N7	1.77598	−0.27414	π*C2–N3	0.00586	48.29	0.28	0.110
LP(1)N8	1.68109	−0.24160	π*N1–C6	−0.0016	64.23	0.24	0.117
			σ*C10–C12	0.4184	5.98	0.66	0.061
			σ*C11–C14	0.4184	6.03	0.66	0.061
LP(1)N9	1.77501	−0.27281	π*C4–N5	−0.00281	49.28	0.27	0.111

The intra-molecular interaction between LP(1)N8 and π*N1–C6 results in larger delocalization with a maximum ΔE_{ij} of 64.23 kcal/mol along with the inter-linkage between lone pair LP(1)N9 and anti-bond π*C4-N5 with ΔE_{ij} of 49.28 kcal/mol between donor-acceptor orbitals [17]. There exists conjugation in DDA-1,3,5T due to π→π* interactions leading to the transfer of charge occurring in the triazine ring between πN1–C6→π*N1–C6, πN1–C6→π*C2–N3, πN1–C6→π*C4–N5, πC2–N3→π*C2–N3, πC2–N3→π*C4–N5, and πC4–N5→π*N1–C6 [18]. Thus, such conjugation and the intensive interaction around the triazine ring leads to bioactivity in DDA-1,3,5T.

3.3 Local Reactivity Descriptors

Fukui functions help in predicting the preferred chemical selectivity and reactivity sites such as electrophilic and nucleophilic sites of an individual atom in a compound [19]. It is a dimensionless quantity. The condensed Fukui functions for different reactivity sites are listed below:

For the nucleophilic attack, $f_j^{+} = q_j(N+1) - q_j(N)$

For an electrophilic attack, $f_j^{-} = q_j(N) - q_j(N-1)$

For radical attack, $f_j^{0} = 1/2[q_j(N+1) - q_j(N-1)]$

where q_j is the charge on the atom at jth level; N, N+1, N−1 are the number of electrons in the neutral, anionic, and cationic states respectively [20]. The condensed dual descriptor $\Delta f(r)$ is expressed as

$$\Delta f(r) = [f^{+} - f^{-}]$$

For attack by nucleophiles, $\Delta f(r) > 0$ whereas $\Delta f(r) < 0$ favours electrophilic attack [21].

The Fukui functions along with dual descriptors and Hirshfeld charges [q(N), q(N+1),q(N−1)] of DDA-1,3,5T were calculated using the Multiwfn program [12] as elucidated in Table 3 which clearly shows that C12 is most prone to nucleophilic attack with a value of 0.0802 and N8 is dominated by an electrophilic attack of value −0.1328. To sum up, C12>C13>C14>C15>H24>H25>H26 is the order for attack by nucleophiles whereas electrophilic attack gradation is N8>N3>N5>N1>H21>N7 > H23.

Table 3. Hirshfeld charges, condensed Fukui functions [f_j^-, f_j^+, f_j^0], and condensed dual descriptors $\Delta f(r)$ of DDA-1,3,5T {Units used below are "e" (elementary charge)}.

Atom	q(N)	q(N+1)	q(N−1)	f_j^-	f_j^+	f_j^0	$\Delta f(r)$
1(N)	−0.227	−0.2464	−0.172	0.055	0.0194	0.0372	−0.0356
2(C)	0.1438	0.1231	0.1723	0.0285	0.0207	0.0246	−0.0078
3(N)	−0.2485	−0.2935	−0.1458	0.1028	0.0449	0.0738	−0.0578
4(C)	0.143	0.1046	0.1721	0.0291	0.0384	0.0337	0.0093
5(N)	−0.2287	−0.239	−0.1648	0.0639	0.0103	0.0371	−0.0535
6(C)	0.1443	0.1071	0.165	0.0207	0.0372	0.0289	0.0164
7(N)	−0.1504	−0.1745	−0.1123	0.0381	0.0241	0.0311	−0.014
8(N)	−0.0353	−0.0463	0.1086	0.1439	0.011	0.0775	−0.1328
9(N)	−0.1503	−0.1813	−0.1131	0.0372	0.031	0.0341	−0.0062
10(C)	−0.0019	−0.0215	0.019	0.0209	0.0196	0.0202	−0.0013
11(C)	−0.0026	−0.0172	0.0171	0.0198	0.0145	0.0171	−0.0053
12(C)	−0.0329	−0.1197	−0.0263	0.0066	0.0868	0.0467	0.0802
13(C)	−0.0876	−0.2123	−0.0322	0.0554	0.1247	0.09	0.0693
14(C)	−0.038	−0.0863	−0.0314	0.0065	0.0483	0.0274	0.0418
15(C)	−0.0852	−0.168	−0.0358	0.0494	0.0828	0.0661	0.0334
16(H)	0.1262	0.11	0.1482	0.0221	0.0162	0.0191	−0.0059
17(H)	0.1263	0.1065	0.1515	0.0252	0.0198	0.0225	−0.0054
18(H)	0.1262	0.1069	0.1488	0.0226	0.0193	0.021	−0.0034
19(H)	0.1266	0.1011	0.1518	0.0251	0.0255	0.0253	0.0004
20(H)	0.0346	0.0098	0.0537	0.0191	0.0248	0.0219	0.0057
21(H)	0.0337	0.0168	0.0656	0.0318	0.0169	0.0244	−0.0149
22(H)	0.0341	0.0176	0.0563	0.0222	0.0165	0.0194	−0.0057
23(H)	0.0318	0.0168	0.0581	0.0263	0.015	0.0206	−0.0113
24(H)	0.0392	0.0016	0.0508	0.0116	0.0376	0.0246	0.026
25(H)	0.0339	−0.0134	0.0566	0.0227	0.0474	0.035	0.0247
26(H)	0.0381	−0.0141	0.0687	0.0306	0.0522	0.0414	0.0215
27(H)	0.0336	0.0101	0.0475	0.014	0.0235	0.0187	0.0095
28(H)	0.0362	0.0027	0.0551	0.0189	0.0335	0.0262	0.0146
29(H)	0.0368	−0.0013	0.0669	0.0301	0.0381	0.0341	0.008

3.4 Wave function Analysis: Electron Localisation Function (ELF) and Localized Orbital Locator (LOL)

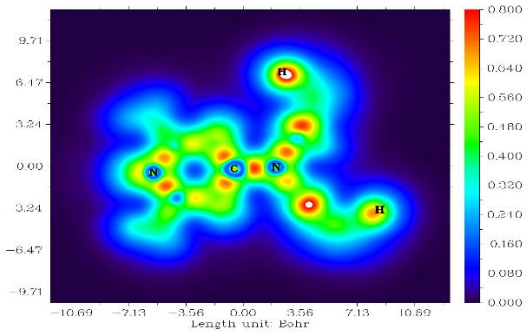

Figure 2. Coloured LOL surface of the DDA-1,3,5T molecule.

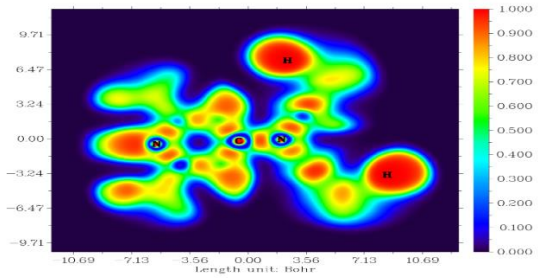

Figure 3. Coloured ELF surface of the DDA-1,3,5T molecule.

The topological characteristics of an electron can be studied using Electron Localisation Function (ELF) and Localized Orbital Locator (LOL). ELF can be understood using the theory of Pauli's repulsion. If the value of ELF approaches one then the Pauli repulsion is maximum and if ELF becomes zero then we get minimum Pauli repulsion [22]. The colourful maps of LOL and ELF of DDA-1,3,5T have been obtained using the Multiwfn program [12] and are depicted in Figure 2 and Figure 3 respectively. Dark blue circles i.e. low ELF values around nitrogen and carbon depict the depleted electronic region between the shells. High ELF red coloured circles tell about the presence of atomic nucleus and high localized electrons due to maximum Pauli repulsion [19,23]. The electron depletion region in LOL is shown in blue encasing carbon and nitrogen. The red colour around carbon and nitrogen in LOL signifies the presence of covalent interactions in that area. The white colour around hydrogen represents high electron density in that region [24].

3.5 Reduced Density Gradient (RDG) analysis

Reduced density gradient *S(r)* is a tool that enables us to comprehend the non-covalent interactions using the concept of electron density gradient $\nabla\rho(r)$ through graphical visualization [25,26]. Both *S(r)*

and $\nabla\rho(r)$ are related to each other and can be expressed as

$$S(r) = \frac{|\nabla\rho(r)|}{2(3\pi)^{\frac{1}{3}}\rho(r)^{\frac{4}{3}}}$$

It is a dimensionless quantity. Non-covalent interactions of DDA-1,3,5T were studied using Multiwfn[12] and the VMD program[13].

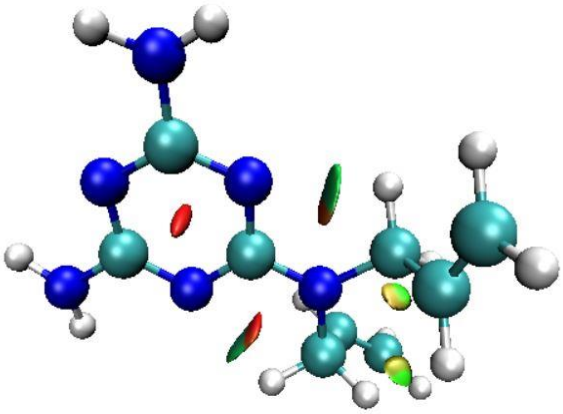

Figure 4. Isosurface of the DDA-1,3,5T molecule in three dimensions.

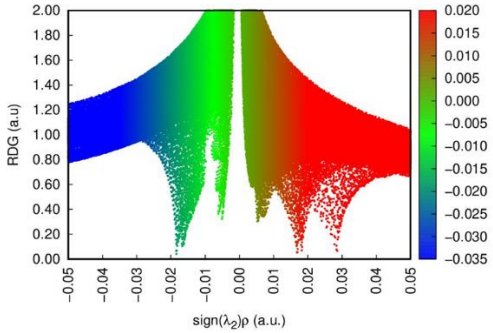

Figure 5. Reduced density gradient scatter plot of the DDA-1,3,5T molecule.

The is surface and the scatter plot (RDG *vs* sign(λ_2)ρ) of DDA-1,3,5T are illustrated in Figure 4 and Figure 5 respectively. Here (λ_2)ρ is the second derivative of the density of the electrons of the Hessian matrix. $\lambda_2<0$ indicates bonding and strong attractive interactions (represented by blue colour) whereas $\lambda_2>0$ represents non-bonding and strong repulsive interactions giving rise to steric effect in rings (represented by red colour). $\lambda_2\approx0$ corresponds to weakly interactive regions namely van der Waals forces and such region is shown in green. Non-covalent interactions are characterized by weak, low reduced gradient and low-density regions. The Laplacian for this region is positive while for covalent interactions, the Laplacian is negative [25,27].

3.6 Molecular Electrostatic Potential (MESP) and Surface Contour

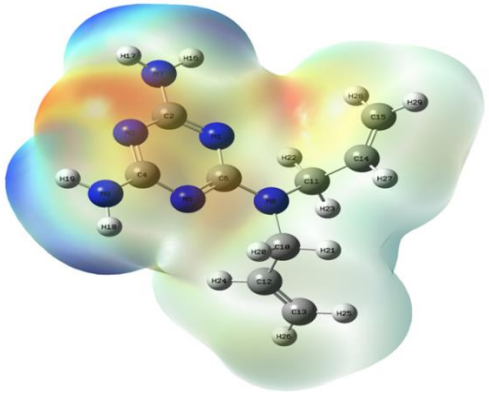

Figure 6. MESP surface of the DDA-1,3,5T molecule.

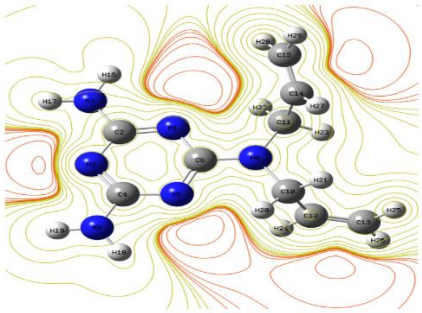

Figure 7. Contour surface of the DDA-1,3,5T molecule.

MEP gives an insight into molecular electronic distribution. It helps in understanding the chemical reactivity, H-bonding sites, electron density and in identifying the nucleophilic and electrophilic attacking sites. The red region represents negative electrostatic potential which is susceptible to attack by an electrophile while the blue region represents positive electrostatic potential susceptible to attack by the nucleophiles [19,28]. The MESP of DDA-1,3,5T lies within the range of -3.981×10^{-2} to 3.981×10^{-2} a.u. along with its contour was computed at 6-311++G(d,p) as illustrated in the Figure 6 and Figure 7. The red region around N3, N7, and N1 is indicative of an electrophilic attack. The blue region around H16, H17, H18, and H19 is dominated by the nucleophilic attack. Yellow lines around hydrogen and carbon in the contour map signify scarcity of electrons while the red lines around electronegative atom nitrogen indicate that this region is rich in electrons.

4. Conclusion

The computational details of the DDA-1,3,5T molecule have been reported for the first time. The bond angle and the bond length have been calculated which matches with the literature. The

ELF-LOL, RDG, NLO, Fukui Indices, confirmed that the compound is stable and chemically reactive. The reduced density gradient investigations of DDA-1,3,5T proved the steric effect in the triazine ring. Fukui indices and MESP study show that the nitrogen atoms in the DDA-1,3,5T molecule are prone to electrophilic attack while the space surrounding the hydrogen and carbon atoms is attacked by the nucleophiles. There exists charge conjugation in DDA-1,3,5T due to $\pi \rightarrow \pi^*$ interactions leading to the transfer of charge occurring in the triazine ring between πN1–C6$\rightarrow\pi^*$N1–C6, πN1–C6$\rightarrow\pi^*$C2–N3, πN1–C6$\rightarrow\pi^*$C4–N5, πC2–N3$\rightarrow\pi^*$C2–N3, πC2–N3$\rightarrow\pi^*$C4–N5, and πC4–N5$\rightarrow\pi^*$N1–C6 which confirms the biological activity of the compound.

Thus, it can be concluded that the DDA-1,3,5T molecule is a stable molecule having potential to be used in the field of medicines.

References

1. G. Zhang, W. Wu, M. Yao, Z. Wu, Y. Jiao, H. Qu, Novel triazine-based metal-organic frameworks: synthesis and mulifunctional application of flame retardant, smoke suppression and toxic attenuation on EP, Mater. Des. 226 (2023) 1–8. https://doi.org/10.1016/j.matdes.2023.111664.
2. X. Li, L. Zhang, S. Niu, Z. Dong, C. Lyu, Quantitatively regulating the ketone structure of triazine-based covalent organic frameworks for efficient visible-light photocatalytic degradation of organic pollutants: Tunable performance and mechanisms, J. Hazard. Mater. 444 (2023). https://doi.org/10.1016/J.JHAZMAT.2022.130366.
3. G. Giacomelli, A. Porcheddu, L. Luca, [1,3,5]-Triazine: A Versatile Heterocycle in Current Applications of Organic Chemistry, Curr. Org. Chem. 8 (2005) 1497–1519. https://doi.org/10.2174/1385272043369845.
4. Z. Zhao, S. Lin, Z. Yu, M. Su, B. Liang, S.X. Liang, X.H. Ju, Facile synthesis of triazine-based microporous organic network for high-efficient adsorption of flumequine and nadifloxacin: A comprehensive study on adsorption mechanisms and practical application potentials, Chemosphere. 315 (2023). https://doi.org/10.1016/J.CHEMOSPHERE.2022.137731.
5. N. Akram, A. Mansha, R. Premkumar, A.M. Franklin Benial, S. Asim, S.Z. Iqbal, H.S. Ali, Spectroscopic, quantum chemical and molecular docking studies on 2,4-dimethoxy-1,3,5-triazine: a potent inhibitor of protein kinase CK2 for the development of breast cancer drug, Mol. Simul. 46 (2020) 1340–1353. https://doi.org/10.1080/08927022.2020.1822526.
6. M.S. Raghu, C.B.P. Kumar, M.K. Prashanth, K.Y. Kumar, Novel 1,3,5-triazine-based pyrazole derivatives as potential antitumor agents and EFGR kinase inhibitors: synthesis, cytotoxicity, DNA binding, molecular docking and DFT studies, (2021) 13909–13924. https://doi.org/10.1039/d1nj02419a.
7. M. Manachou, Z. Gouid, Z. Almi, S. Belaidi, S. Boughdiri, M. Manachou, Z. Gouid, Z. Almi, S. Belaidi, S. Boughdiri, Pyrazolo[1,5-a][1,3,5]triazin-2-thioxo-4-ones derivatives as thymidine phosphorylase inhibitors: Structure, drug-like calculations and quantitative structure-activity relationships (QSAR) modeling To cite this version : HAL Id : hal-02974009, J. Mol. Struct. 1199 (2021) 22. https://doi.org/10.1016/j.molstruc.2019.127027.
8. M. Chalermnon, C. Sarocha, A. Sereemaspun, R. Rojanathanes, T. Khotavivattana, Biguanide -Based Synthesis of 1,3,5-Triazine Derivatives with Anticancer Activity and 1,3,5-Triazine Incorporated Calcium Citrate Nanoparticles, Molecules. 26 (2021) 1–14. https://doi.org/https://doi.org/10.3390/molecules26041028.
9. V.M. Vidya, P. Chetti, Linear and non-linear optical characteristics of some 1 , 3 , 5-triazines influenced by prototropic tautomerism : A DFT study, Opt. Mater. (Amst). 109 (2020) 110365. https://doi.org/10.1016/j.optmat.2020.110365.
10. M.J. Frisch, G.W. Trucks, H.B. Schlegel, G.E. Scuseria, M.A. Robb, J.R. Cheeseman, G. Scalmani, V. Barone, B. Mennucci, G.A. Petersson, H. Nakatsuji, M. Caricato, X. Li, H.P. Hratchian, A.F. Izmaylov, J. Bloino, G. Zheng, J.L. Sonnenberg, M. Hada, M. Ehara, K. Toyota, R. Fukuda, J. Hasegawa, M. Ishida, T. Nakajima, Y. Honda, O. Kitao, H. Nakai, T. Vreven, J.A. Montgomery, J.E. Peralta, F. Ogliaro, M. Bearpark, J.J. Heyd, E. Brothers, K.N. Kudin, V.N. Staroverov, R. Kobayashi, J. Normand, K. Raghavachari, A. Rendell, J.C. Burant, S.S. Iyengar, J. Tomasi, M. Cossi, N. Rega, J.M. Millam, M. Klene, J.E. Knox, J.B. Cross, V. Bakken, C. Adamo, J. Jaramillo, R. Gomperts, R.E. Stratmann, O. Yazyev, A.J. Austin, R. Cammi, C. Pomelli, J.W. Ochterski, R.L. Martin, K. Morokuma, V.G. Zakrzewski,

G.A. Voth, P. Salvador, J.J. Dannenberg, S. Dapprich, A.D. Daniels, Ö. Farkas, J.B. Foresman, J. V. Ortiz, J. Cioslowski, D.J. Fox, Gaussian09, Gaussian 09. (2009).
11. 2016. GaussView, Version 6, Dennington, Roy; Keith, Todd A.; Millam, John M. Semichem Inc., Shawnee Mission, KS, GaussView 6, Gaussian. (2016).
12. T. Lu, F. Chen, Multiwfn: A multifunctional wavefunction analyzer, J. Comput. Chem. 33 (2012) 580–592. https://doi.org/10.1002/jcc.22885.
13. W. Humphrey, A. Dalke, K. Schulten, VMD: Visual Molecular Dynamics, J. Mol. Graph. (1996).
14. J. Teotia, Annu, I. Rathi, S. Bhardwaj, R.K. Uppadhayay, A. Garg, Vibrational (FT-IR and FT-Raman) Spectroscopic Investigations , NLO , NBO and MEP Analysis by DFT, in: Proc. Int. Conf. At. Mol. Opt. Nano Phys. with Appl., Springer Singapore, 2022: pp. 439–462. https://doi.org/10.1007/978-981-16-7691-8.
15. S. Muthu, A. Prabhakaran, Vibrational spectroscopic study and NBO analysis on tranexamic acid using DFT method, Spectrochim. Acta - Part A Mol. Biomol. Spectrosc. 129 (2014) 184–192. https://doi.org/10.1016/j.saa.2014.03.050.
16. V. Arjunan, S. Thirunarayanan, S. Mohan, Energy profile, spectroscopic (FT–IR, FT–Raman and FT–NMR) and DFT studies of 4–bromoisophthalic acid, J. Mol. Struct. (2018). https://doi.org/10.1016/j.molstruc.2017.12.032.
17. T. Beena, L. Sudha, A. Nataraj, V. Balachandran, D. Kannan, M.N. Ponnuswamy, Synthesis, spectroscopic, dielectric, molecular docking and DFT studies of (3E)-3-(4-methylbenzylidene)-3,4-dihydro_2H-chromen-2-one: an anticancer, Chem. Cent. J. 11 (2017) 1–19. https://doi.org/10.1186/s13065-016-0230-8.
18. M. Khalid, M.A. Ullah, M. Adeel, M. Usman Khan, M.N. Tahir, A.A.C. Braga, Synthesis, crystal structure analysis, spectral IR, UV–Vis, NMR assessments, electronic and nonlinear optical properties of potent quinoline based derivatives: Interplay of experimental and DFT study, J. Saudi Chem. Soc. 23 (2019) 546–560. https://doi.org/10.1016/j.jscs.2018.09.006.
19. S. Sevvanthi, S. Muthu, S. Aayisha, P. Ramesh, M. Raja, Spectroscopic (FT-IR, FT-Raman and UV-Vis), computational (ELF, LOL, NBO, HOMO-LUMO, Fukui, MEP) studies and molecular docking on benzodiazepine derivatives-heterocyclic organic arenes, Chem. Data Collect. 30 (2020) 100574. https://doi.org/10.1016/j.cdc.2020.100574.
20. S. Saravanan, V. Balachandran, Quantum mechanical study and spectroscopic (FT-IR, FT-Raman, UV-Visible) study, potential energy surface scan, Fukui function analysis and HOMO-LUMO analysis of 3-tert-butyl-4-methoxyphenol by DFT methods, Spectrochim. Acta - Part A Mol. Biomol. Spectrosc. 130 (2014) 604–620. https://doi.org/10.1016/j.saa.2014.04.058.
21. J. Padmanabhan, R. Parthasarathi, M. Elango, V. Subramanian, B.S. Krishnamoorthy, S. Gutierrez-Oliva, A. Toro-Labbé, D.R. Roy, P.K. Chattaraj, Multiphilic descriptor for chemical reactivity and selectivity, J. Phys. Chem. A. 111 (2007) 9130–9138. https://doi.org/10.1021/jp0718909.
22. J. George, J.C. Prasana, S. Muthu, T.K. Kuruvilla, S. Sevanthi, R.S. Saji, Spectroscopic (FT-IR, FT Raman) and quantum mechanical study on N-(2,6-dimethylphenyl)-2-{4-[2-hydroxy-3-(2-methoxyphenoxy)propyl]piperazin-1-yl} aceta mide, J. Mol. Struct. 1171 (2018) 268–278. https://doi.org/10.1016/j.molstruc.2018.05.106.
23. R.S. Saji, J.C. Prasana, S. Muthu, J. George, T.K. Kuruvilla, B.R. Raajaraman, Spectros copic and quantum computational study on naproxen sodium, Spectrochim. Acta - Part A Mol. Biomol. Spectrosc. 226 (2020) 117614. https://doi.org/10.1016/j.saa.2019.117614.
24. A. Saral, P. Sudha, S. Muthu, S. Sevvanthi, P. Sangeetha, S. Selvakumari, Vibrational spectroscopy, quantum computational and molecular docking studies on 2-chloroquinoline-3-carboxaldehyde, Heliyon. 7 (2021) 1–15. https://doi.org/10.1016/j.heliyon.2021.e07529.
25. E.R. Johnson, S. Keinan, P. Mori-Sánchez, J. Contreras-García, A.J. Cohen, W. Yang, Revealing noncovalent interactions, J. Am. Chem. Soc. 132 (2010) 6498–6506. https://doi.org/10.1021/ja100936w.
26. M.C. Sekhar, D. Wakgiri, D.N. Kenie, Study of Intermolecular Interactions between 2-Chloroaniline Isomeric Butanol Complexes in Gas Phase by Using DFT, NBO, QTAIM and RDG Analysis M.CHANDRA, Asian J. Chem. 31 (2019) 538–544. https://doi.org/10.14233/ajchem.2019.21651.
27. K. Vanasundari, V. Balachandran, M. Kavimani, B. Narayana, Molecular docking, vibrational, structural, electronic and optical studies of {4 – (2, 6) dichlorophenyl amino 2 –

methylidene 4 – oxobutanoic acid and 4- (2, 5)} dichlorophenyl amino 2 – methylidene 4 – oxobutanoic acid – A comparative study, J. Mol. Struct. 1155 (2018) 21–38. https://doi.org/10.1016/j.molstruc.2017.11.002.

28. K. Singh, I. bala, R. Kataria, Crystal structure, Hirshfeld surface and DFT based NBO, NLO, ECT and MEP of benzothiazole based hydrazone, Chem. Phys. 538 (2020) 110873. https://doi.org/10.1016/j.chemphys.2020.110873.